

# Synergistic Effect of Dual-Anion Additives Promotes the Fast Dynamics and High-Voltage Performance of Ni-Rich Lithium-Ion Batteries by Regulating the Electrode/Electrolyte Interface

Pengpeng Dai, Xiangbang Kong, Huiya Yang, Silan Kuang, Jing Zeng, and Jinbao Zhao\*



Cite This: <https://doi.org/10.1021/acsami.2c08724>



Read Online

ACCESS |



Metrics & More



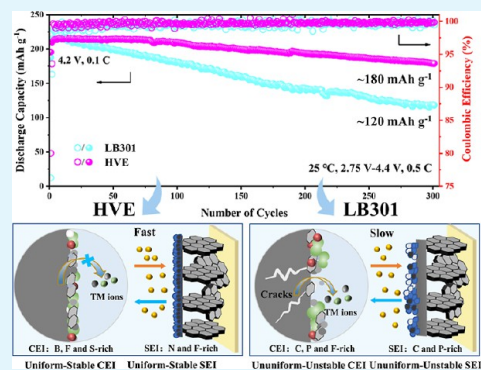
Article Recommendations



Supporting Information

**ABSTRACT:** Combining the Ni-rich layered cathode ( $\text{Ni} \geq 80\%$ ) with high operating voltage is considered as a feasible solution to achieve high-energy lithium-ion batteries (LIBs). However, the working voltage is limited in practical applications due to the poor interface stability in traditional carbonate electrolytes. Herein,  $\text{LiBF}_4$  and  $\text{LiNO}_3$  are added as film-forming additives and 1.0 M  $\text{LiPF}_6$  in SL/FEC/EMC with 0.5 wt %  $\text{LiBF}_4\text{-LiNO}_3$  (HVE) is obtained. A uniform and inorganic-rich cathode electrolyte interphase (CEI) as well as a dense and  $\text{Li}_3\text{N-LiF}$ -rich solid electrolyte interphase (SEI) could be in situ generated on  $\text{LiNi}_{0.8}\text{Co}_{0.1}\text{Mn}_{0.1}\text{O}_2$  (NCM811) and graphite (Gr) electrode in HVE, respectively. The robust interface film with electronic insulation and ionic conductivity effectively stabilizes the NCM811/Gr-electrolyte interfaces and improves the  $\text{Li}^+$  diffusion kinetics, enabling the high-load NCM811-Gr to maintain 85.2% capacity ( $\sim 180 \text{ mA h g}^{-1}$ ) after 300 cycles under 4.4 V. Besides, the 4.2 V NCM811-Gr retains 90.4% of the initial capacity after 200 cycles at 2 C ( $\sim 6 \text{ mA h cm}^{-2}$ ). Compared with the traditional carbonate electrolyte (LB301), HVE has obvious advantages in terms of high-voltage and fast dynamics performance. Especially, good thermal stability and economy make HVE a promising electrolyte for commercial high-energy LIBs.

**KEYWORDS:** additive, electrolyte, interface, high voltage, fast dynamics, NCM811-Gr LIBs



## 1. INTRODUCTION

Due to the ever-increasing market requirements for high-energy LIBs, the use of Ni-rich layered cathode ( $\text{Ni} \geq 80\%$ ) and high operating voltage are considered as feasible solutions.<sup>1,2</sup> High-capacity LIBs can be obtained by combining NCM811 with Gr. However, the operating voltage is limited to below 4.3 V (*vs*  $\text{Li/Li}^+$ ) in practical applications due to the limitation of traditional carbonate electrolytes.<sup>1–3</sup> Apart from the decomposition of the electrolyte, the increase in cutoff voltage would cause structural degradation of NCM811 and side reactions with electrolyte, including detrimental phase transitions, transition metal (TM) dissolution, and micro-cracks.<sup>4–7</sup> This severe degradation would lead to a rapid increase in impedance and irreversible capacity during cycling.<sup>8–10</sup> Also, the dissolved TM ion can migrate and deposit on Gr, causing the consumption of active Li, the deterioration of solid electrolyte interphase (SEI), and the significant increase in impedance, which further accelerates the performance failure of LIBs.<sup>6</sup>

Various efforts have been made to protect the cathode from structural degradation under high voltage.<sup>11–15</sup> Studies reveal that cathode electrolyte interphase (CEI) is the key to the performance stability of LIBs.<sup>11,15,16</sup> In traditional carbonate electrolytes, the uneven and unstable CEI with poor mechanical/chemical stability and low ionic conductivity

would lead to continuous decomposition and regeneration under high voltage.<sup>17</sup> In situ formation of a robust CEI is expected to be an important way to suppress the degradation of NCM811.<sup>18</sup> Although Gr is more stable than NCM811, TM migration to Gr becomes more severe under high voltage, which is also the main reason for the performance fading of LIBs.<sup>6,19</sup> Thus, the design of effective SEI is as crucial as CEI for the cycle life of LIBs under high voltage. Decomposition of carbonate electrolytes and serious parasitic reactions at the electrode–electrolyte interface under high voltage are the main reasons for the poor quality of CEI and SEI.<sup>20,21</sup> The existing strategies for the performance degradation of the full battery under high voltage mainly focus on individual modification of the positive electrode or the negative electrode side, and the experimental electrode used in many published literature have low loadings, which are difficult to truly reveal and solve the problems in practical applications.<sup>14,16,22–24</sup> Therefore, it is of

Received: May 16, 2022

Accepted: August 15, 2022

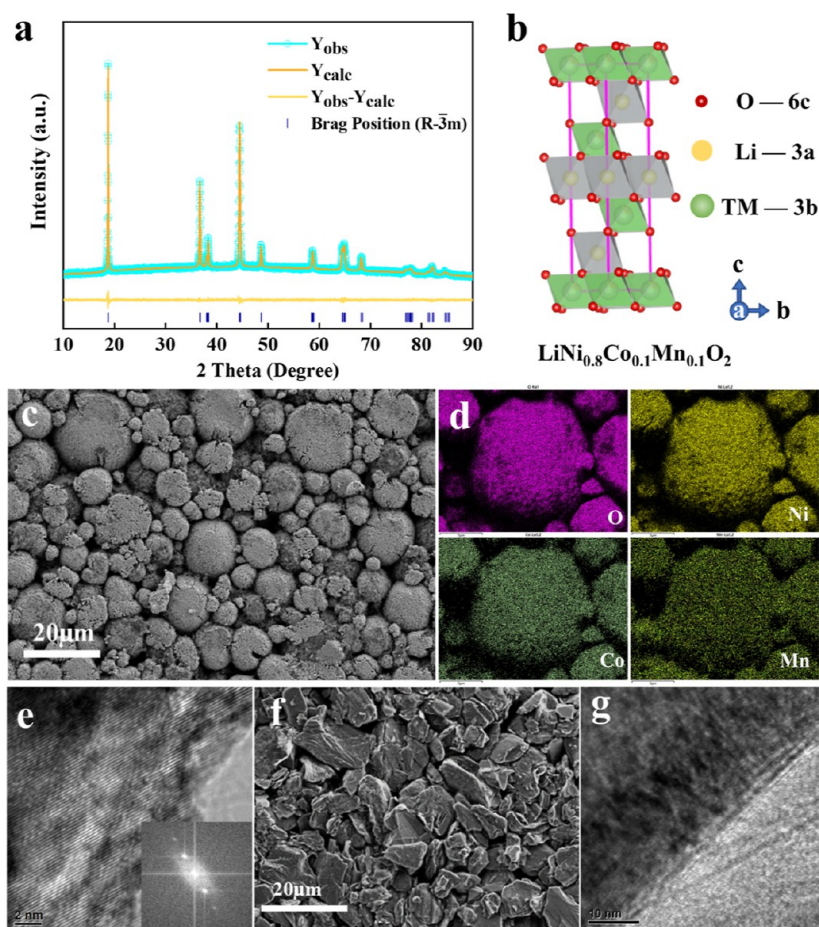


**Figure 1.** Structure and morphology of NCM811 and Gr. (a) Rietveld refinement of the XRD pattern of pristine NCM811; (b) structural model of NCM811; (c) SEM of NCM811 and (d) its elemental mappings; (e) TEM of NCM811; (f) SEM and (g) TEM of Gr.

great practical significance to develop a high-voltage electrolyte suitable for commercial high-load NCM811-Gr LIBs.

LiPF<sub>6</sub> is a commonly used and cheap lithium salt with good comprehensive properties.<sup>25</sup> FEC has higher oxidation stability and ideal SEI formation effect.<sup>26</sup> SL with high dielectric constant and oxidation potential over 5.8 V (*vs* Li/Li<sup>+</sup>) can form a protective film on the positive electrode.<sup>27</sup> EMC is used to reduce the viscosity. FEC, SL, and low-viscosity carbonate systems have been used in high-voltage electrolytes but have limited protection for NCM811-Gr, especially under high voltage.<sup>28,29</sup> The use of additives for interface modification is as vital as the choice of solvent to improve the high-voltage performance.<sup>30</sup> LiNO<sub>3</sub> can be reduced to form a strong SEI (lithium-nitrogen compound with fast ion conductivity) to stabilize the negative electrode,<sup>31</sup> and LiBF<sub>4</sub> can improve the cycling stability of the positive electrode by reducing the impedance.<sup>32,33</sup> Thus, LiNO<sub>3</sub>-LiBF<sub>4</sub> are selected as dual additives to synergistically enhance the property of the electrolyte. Considering the viscosity and electrochemical performance, the electrolyte was prepared as follows after preliminary experiments: 1.0 M LiPF<sub>6</sub> dissolved in SL/FEC/EMC (1:1:3, *v/v/v*) with 0.5 wt % LiBF<sub>4</sub>-LiNO<sub>3</sub>.

In summary, the addition of LiBF<sub>4</sub> and LiNO<sub>3</sub> as dual additives in SL/FEC/EMC results in the formation of a uniform and LiF-inorganic (including B and S)-rich CEI and a dense, thin, and Li<sub>3</sub>N-LiF-rich SEI. Theoretical calculation and characterizations show that additives can synergistically stabilize the electrode-electrolyte interfaces. This work

demonstrates that the synergistic regulation of BF<sub>4</sub><sup>-</sup>-NO<sub>3</sub><sup>-</sup> dianion additives in the high-voltage electrolyte system to generate CEI and SEI with electronic insulation and ionic conductivity properties can improve the stability of NCM811-Gr under high voltage, providing an operational and economic strategy to design high-voltage electrolytes for commercial high-energy LIBs with an outstanding performance.

## 2. EXPERIMENTAL SECTION

**2.1. Preparation of Materials.** LB301 was used as a comparison sample and prepared by evenly mixing ethylene carbonate (EC) and dimethyl carbonate (DMC) in a volume ratio of 1:1 with 1.0 M LiPF<sub>6</sub>. SL, FEC, and EMC were evenly mixed in a volume ratio of 1:1:3 with 1.0 M LiPF<sub>6</sub> (and additives) to prepare high-voltage electrolytes. The prepared electrolytes were obtained after stirring for 10 h at 50 °C. For the convenience of expression, the four high-voltage electrolytes (no additive, 0.5 wt % LiNO<sub>3</sub>, 0.5 wt % LiBF<sub>4</sub>, and 0.5 wt % LiNO<sub>3</sub> with 0.5 wt % LiBF<sub>4</sub> dual additives) were labeled as SL/FEC/EMC, LNO-SL/FEC/EMC, LBF-SL/FEC/EMC, and HVE, respectively. The above-mentioned solvent and lithium salt were provided by Zhangjiagang Guotai Huarong New Chemical Materials Co., Ltd. The NCM811 and Gr electrodes used in this study were provided by Tianjin JEVE Power Co., Ltd. The composition of the positive electrode includes NCM811 (97.35 wt %), SuperP, and poly(vinylidene difluoride), and the negative electrode is composed of Gr (95.7 wt %), SuperP, CMC, and SBR. The loading of the NCM811 electrode is about 20 mg·cm<sup>-2</sup>, and the N/P ratio is about 1.10.

**2.2. Theoretical Calculation.** The DFT (density functional theory) calculation of the lowest unoccupied molecular orbital

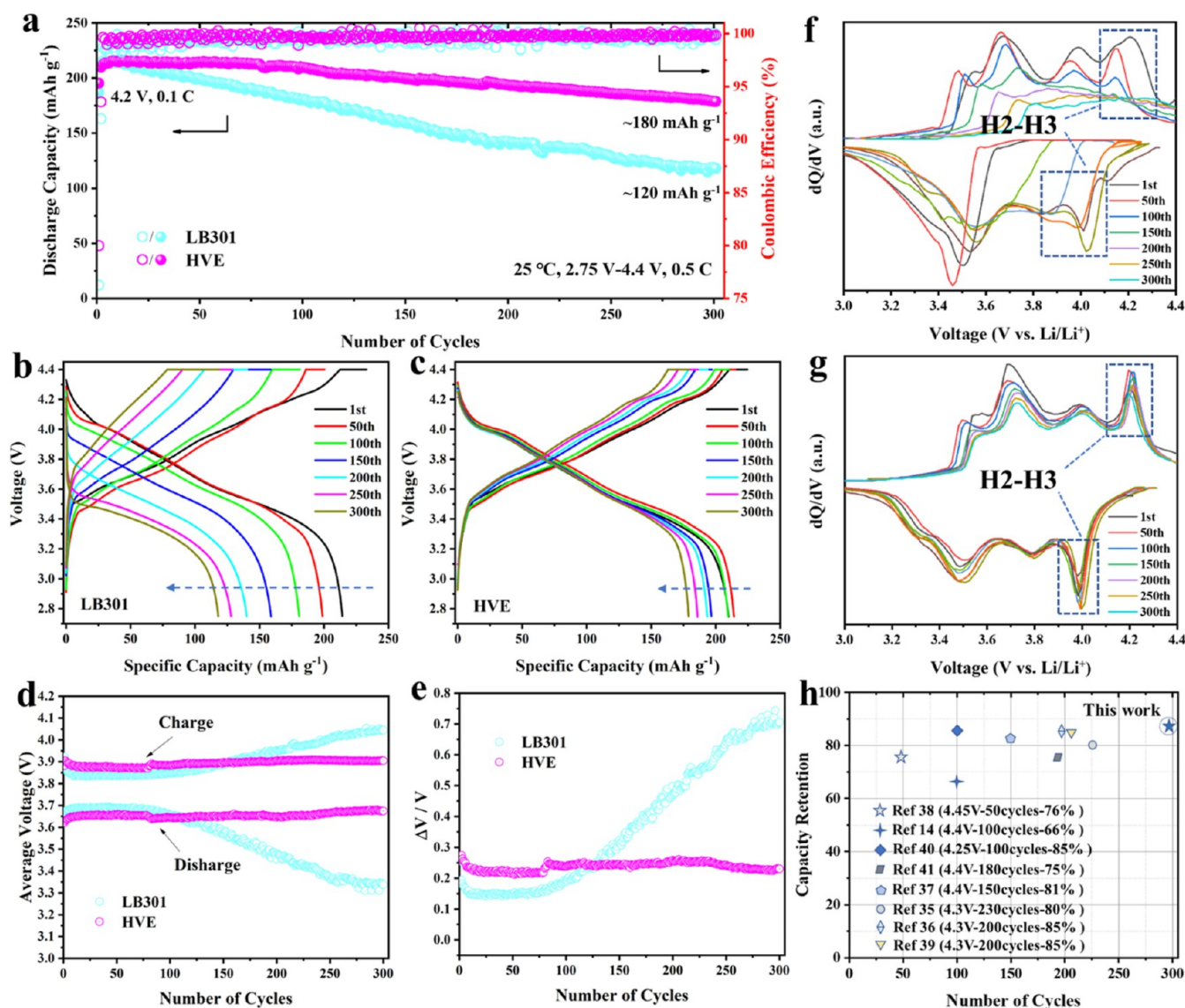


**Figure 2.** Electrochemical performance of NCM811-Gr cells employing LB301 and HVE. (a) Galvanostatic cycling; (b,c) selected charge–discharge profiles for the 300 cycles; (d) average charge/discharge voltage curves and (e) average voltage hysteresis ( $\Delta V$ ) upon cycling; and (f,g) corresponding  $dQ/dV$  curves of (b,c); (h) comparison of the electrochemical performance of this study with other works.<sup>14,35–41</sup>

(LUMO) in this study was conducted on the Gaussian 09 software package. The B3LYP42 method at the 6-311+G (d, p) basis set was used to optimize the geometry structure.<sup>34</sup>

**2.3. Electrochemical Measurements and Materials Characterizations.** The above-mentioned electrodes, Asahi Kasei polyethylene separator, and LB301 or the prepared high-voltage electrolytes were used to assemble CR2016 coin cells in the Ar-glovebox. Electrochemical performance was tested by Neware battery test instrument under the working voltage of 2.75–4.2/4.4 V at 25 °C (1 C = 180 mA g<sup>-1</sup>). Linear sweep voltammetry (LSV, 3.0–5.0 V, 1 mV s<sup>-1</sup>) tests of the electrolytes were conducted on an electrochemical workstation (CHI660E) by using a three-electrode system. The working electrode was an Al foil, and Li metal was used as the counter electrode and the reference electrode. An electrochemical workstation (Solartron SI 1287/1260) was used to test the electrochemical impedance spectroscopy (EIS, frequency range: 0.01–10<sup>5</sup> Hz); field-emission scanning electron microscopy (SEM, Zeiss GeminiSEM 500) and energy-dispersive spectroscopy (EDS) mapping were used to observe the morphology and conduct the corresponding elemental analysis of electrodes; X-ray diffraction (XRD, Rigaku Ultima IV) was used to characterize the bulk structure of electrodes; transmission electron microscopy (TEM, FEI Tecnai

F30) was used to study the structure and CEI/SEI of NCM811 and Gr; Raman spectroscopy (Horiba LabRAM HR Evolution) was used to characterize the surface structure change of NCM811 during cycling; X-ray photoelectron spectroscopy (XPS, ThermoScientific ESCALAB Xi+) was used to analyze the surface composition of NCM811 and Gr.

### 3. RESULTS AND DISCUSSION

The physical properties of the positive and negative electrodes are shown in Figure 1. The XRD Rietveld refinement of the pristine NCM811 and the corresponding layered structure model are shown in Figure 1a,b. The results indicate that the pristine NCM811 has a hexagonal layered  $\alpha$ -NaFeO<sub>2</sub> structure (space group:  $R\bar{3}m$ ) and negligible cation mixing ( $w_{Rp} = 2.29\%$ ;  $R_p = 1.73\%$ ;  $CHI = 1.461$ ). The detailed refined atomic parameters are listed in Table S1. SEM (Figure 1c) reveals that NCM811 is in the form of spherical secondary particles with diameters ranging from 10 to 20  $\mu\text{m}$  and consists of primary particles with a diameter of approximately 500 nm (Figure S1a,b). The corresponding EDS elemental mappings (Figure

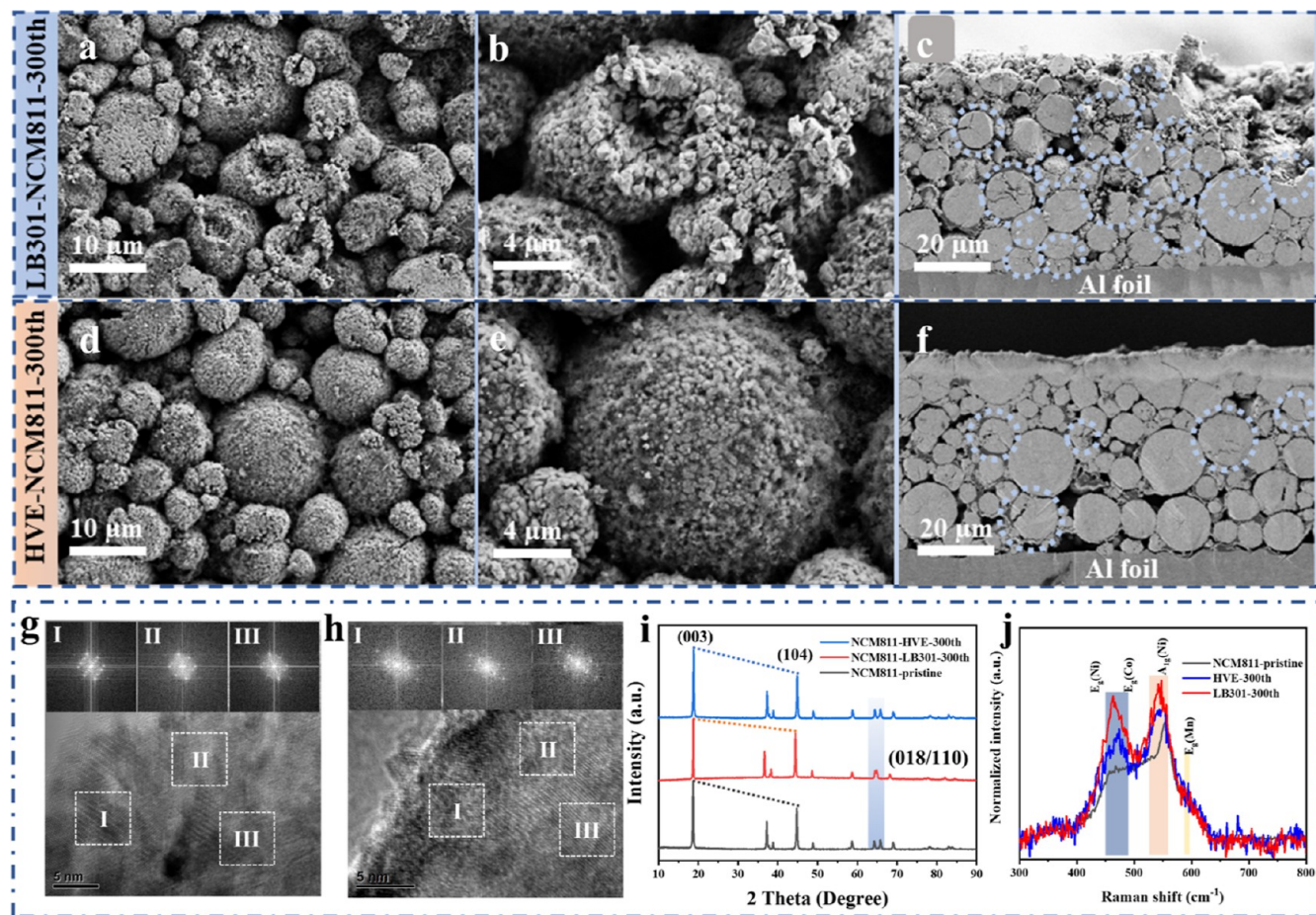


**Figure 3.** SEM and cross-sectional SEM and TEM (inset: corresponding FFT patterns) of NCM811 employing (a–c, g) LB301 and (d–f, h) HVE after 300 cycles under 4.4 V. (i) XRD and (j) Raman test of pristine NCM811 and cycled electrodes in both electrolytes.

1d) show that O and TM (Ni, Co, and Mn) are uniformly distributed on the secondary particles. In addition, it can be seen that there are a few microcracks on the surface of uncycled particles in commercial high-load NCM811 electrode due to rolling (Figure S1a–c). TEM and fast Fourier transform (FFT) (Figure 1e) confirm that the pristine NCM811 has a good layered structure with no rock-salt phase. As shown in Figures 1f,g and S2a,b, the pristine Gr has a clear crystal lattice and smooth surface, indicating a high degree of crystallinity. The positive and negative electrodes are assembled with Li for half-cell electrochemical performance testing, respectively (Figures S1d and S2c). The above-mentioned results indicate that the positive and negative electrode materials used in our study have satisfactory structural and electrochemical properties and will be used to evaluate the electrolytes.

Screening of high-voltage electrolytes is displayed in the Supporting Information (Figures S3–S11). The LSV test results show that the prepared four electrolytes all have high oxidation resistance. The optimal electrolyte was selected by comparing the cycle performance and the integrity of the electrodes after cycling. The prepared four electrolytes in NCM811-Gr all exhibit excellent performance under 4.4 V, and HVE shows the best cycling stability. Finally, we determined HVE as the final high-voltage electrolyte. The electrochemical performance and corresponding characterization compared with LB301 will be studied in the following discussion.

The galvanostatic cycling data of LB301 and HVE under 4.4 V (0.5 C) after 300 cycles are shown in Figure 2a. Specifically, HVE maintained a specific discharge capacity of  $\sim 180$  mA h  $g^{-1}$  after 300 cycles, with a capacity retention of 85.18%. In contrast, the discharge specific capacity of LB301 is  $\sim 118$  mA h  $g^{-1}$ , and the capacity retention is only 55.09% at the same condition. Compared with LB301, the cycling stability of HVE is greatly improved, indicating that the high-voltage electrolyte can alleviate the poor cycling stability of NCM811-Gr cells under high voltage. The charge–discharge curves (Figure 2b,c) and corresponding normalized charge–discharge curves (Figure S12) of LB301 and HVE show that the average charge voltage plateau of LB301 increased continuously, as well as the initial discharge voltage and average discharge voltage plateau decreased sharply during cycling, accompanied by a severe decline in discharge specific capacity. However, the initial discharge voltage and average charge/discharge voltage plateaus of HVE are quite stable with a relatively little discharge capacity decrease during cycling. This suggests that HVE can reduce polarization and alleviate voltage hysteresis (confirmed by Figure S13) under high voltage, thereby stabilizing the electrochemical performance of NCM811-Gr. The average charge and discharge voltages obtained from the charge–discharge curves are shown in Figure 2d. The average charge voltage of LB301 increases rapidly after 100 cycles, indicating a significant increase in polarization. This may be due to the accumulation of resistive surface film on the positive electrode, which is related to the propagation of microcracks

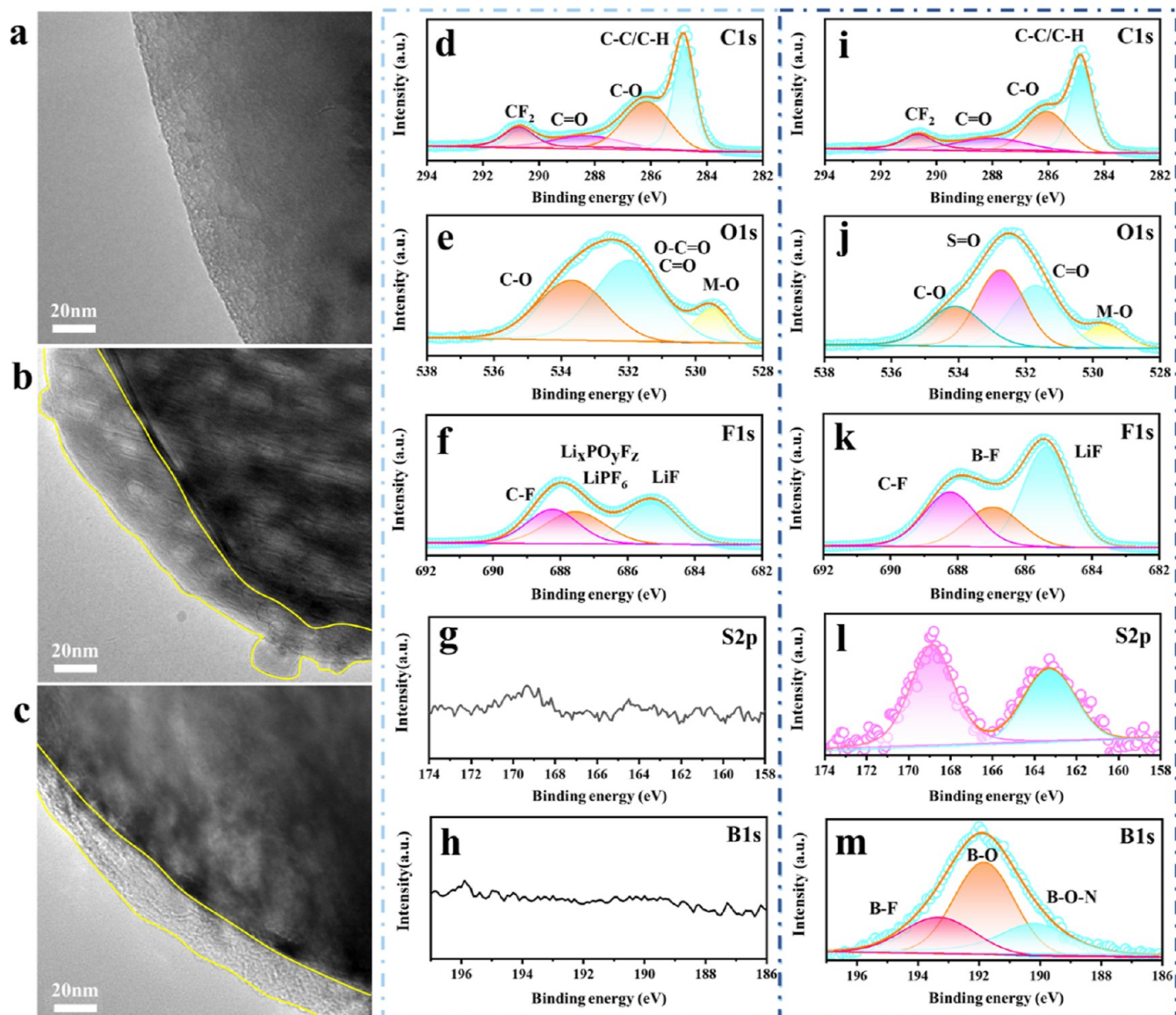


**Figure 4.** TEM of (a) pristine NCM811 and cycled samples in (b) LB301 and (c) HVE. XPS of NCM811 electrodes employing (d–h) LB301 and (i–m) HVE after 300 cycles under 4.4 V.

and violent parasitic reactions with electrolyte in the highly delithiated state.<sup>42</sup> More seriously, the average discharge voltage drops rapidly after 100 cycles, which directly lead to the rapid drop in capacity. In contrast, the average voltage of HVE during charge and discharge is quite stable. The polarization of HVE is initially slightly higher because of the higher viscosity and lower ionic conductivity (Table S2), whereas, the stabilization of the average discharge/charge voltage makes HVE more favorable in terms of energy storage. By subtracting the average discharge voltage from the average charge voltage, the charge curve of the charge–discharge polarization voltage ( $\Delta V$ ) with the number of cycles can be obtained, as shown in Figure 2e. The  $\Delta V$  of HVE sustains a steady line upon cycling, while that of LB301 increases continuously. This may be related to the undamaged NCM811 structure and a less resistive and robust CEI in HVE. Further analysis of  $\Delta V$  is shown in Figure S14, which reveals that the reason for the capacity decay of LB301 mainly comes from the increase of internal resistance and that of HVE is mainly due to the loss of active Li rather than the increase of internal

resistance.<sup>43</sup> The  $dQ/dV$  curves during cycling are also employed to explore the origin of different cycling behaviors of the two electrolytes. As shown in Figure 2f,g, the charge/discharge polarization of LB301 increases rapidly, which is manifested as the position shift of H2–H3 peak during cycling, and the H2–H3 peak intensity decreases rapidly and finally almost disappears. In contrast, the H2–H3 peak of NCM811-Gr in HVE is well-maintained and less polarized after 300 cycles. The oxidation/reduction peaks overlap well during cycling in HVE, indicating the enhanced structural reversibility of the cathode. The above-mentioned experimental phenomenon is due to the different reaction reversibility of NCM811 under high voltage in LB301 and HVE. Compared with LB301, HVE is believed to stabilize the cathode–electrolyte interface and thus enhance the structural reversibility of NCM811, which will be confirmed in the following discussions. The increased polarization is an important reason for the rapid degradation of battery performance.<sup>42</sup> Especially, the NCM811-Gr full cell in our study displays a superior electrochemical performance compared with other

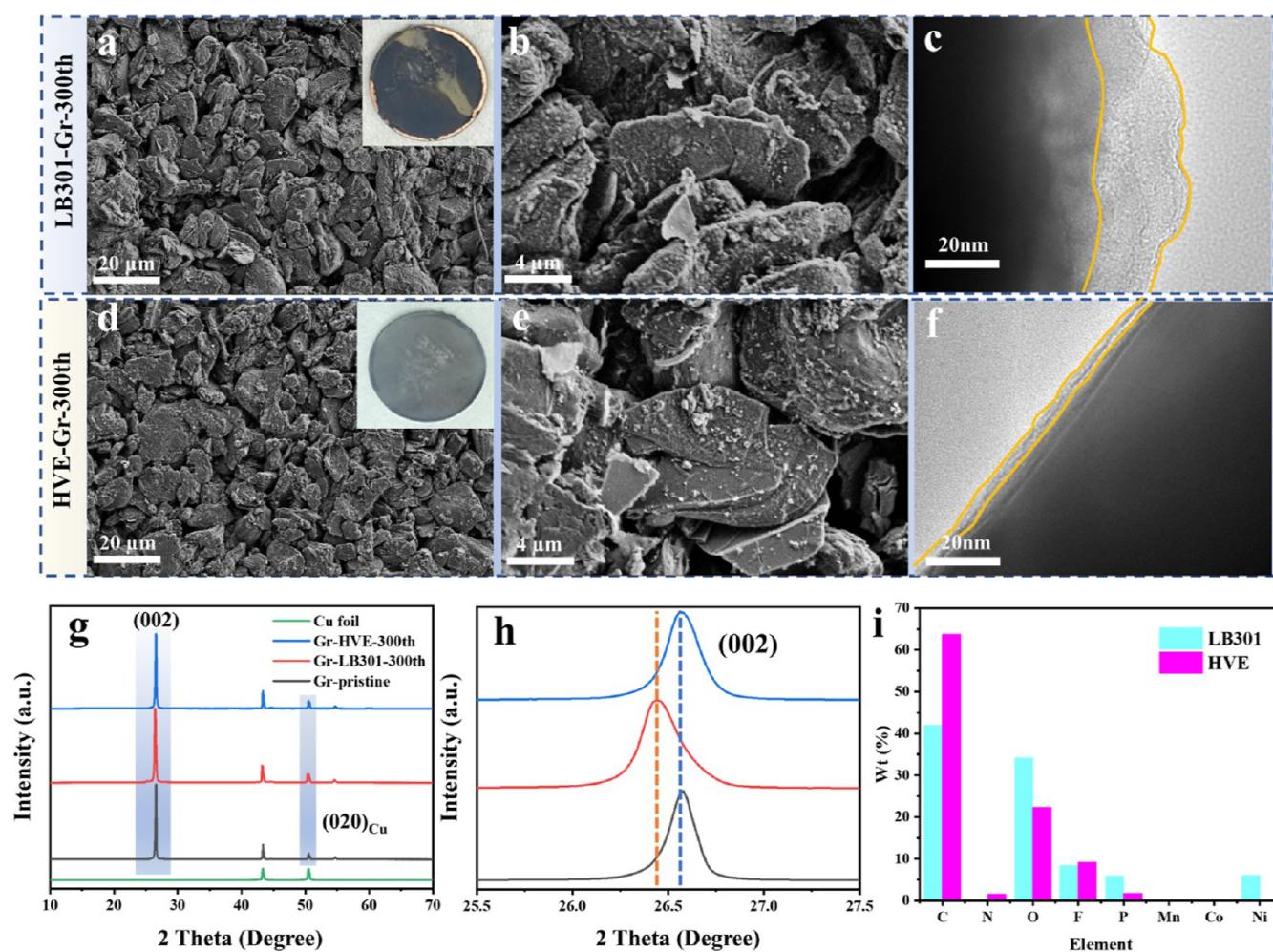


**Figure 5.** SEM, optical photographs, and low-resolution TEM of Gr electrodes employing (a–c) LB301 and (d–f) HVE after 300 cycles under 4.4 V (0.5 C). (g,h) XRD results of cycled electrodes in both electrolytes compared with pristine Gr. (i) Element analysis in EDS results of both cycled Gr samples.

works<sup>14,35–41</sup> (Figure 2h). The above-mentioned results clearly confirm the excellent property of HVE as a high-voltage electrolyte. Considering the economy and property, the prepared HVE is expected to have good commercialization prospects.

Studies have proved that crack and pulverization of the Ni-rich cathode are important reasons for performance degradation.<sup>9,42</sup> Thus, the cells after 300 cycles are disassembled and then soaked and rinsed with DMC. The SEM and cross-sectional SEM images (Figure 3a–c) of NCM811 electrode after cycling in LB301 show that a large number of microcracks and even serious pulverization appear on the surface of NCM811 particles. As shown in Figure 3d–f, cracked secondary particles also appear in HVE, but the number of cracked particles is greatly reduced. Also, the NCM811 electrode after cycling in HVE does not show significant surface pulverization.

The primary particles inside the cracked secondary particles will no longer participate in the redox reaction due to the loss of electrical contact, thus no longer providing capacity. In addition, the electrolyte will gradually penetrate into the interior of the particles with the cracks, which will aggravate the interfacial side reactions and increases the internal resistance, and eventually leads to the deterioration of battery performance. Especially, Ni<sup>4+</sup> will react with the electrolyte and

reduce to Ni<sup>2+</sup> at high state of charge (SOC). Since Ni<sup>2+</sup> (0.69 Å) and Li<sup>+</sup> (0.76 Å) have similar ionic radius, Ni<sup>2+</sup> tends to migrate to the Li layer, resulting in an electrochemically inactive surface phase transition. On combining high-resolution TEM with FFT results (Figure 3g,h), it is found that the disordered surface reconstruction layer (rock-salt phase, Li/TM mixing) on the surface of NCM811 is quite thick (over 30 nm) after cycling in LB301. However, NCM811 showed a more uniform and thinner surface reconstruction layer (5–10 nm) after cycling in HVE. Despite the presence of rock-salt phase and Li/TM mixing, most of the surface area remains as layered structure. Studies have found that the rock-salt phase will strongly hinder the insertion and extraction of Li<sup>+</sup> into the lattice, resulting in a rapid increase in polarization voltage and performance degradation.<sup>8,44</sup> Therefore, it is consistent with the results of the charge–discharge curves and dQ/dV curves.

XRD tests (Figure 3i) are performed on NCM811 after cycling in both electrolytes and compared with the pristine NCM811. It can be seen that all peak shapes of both cycled NCM811 are basically consistent with the pristine NCM811, which means the overall layered structure does not change. The intensity ratio of (003)/(104) peaks and the splitting degree of the (018)/(110) peaks of NCM811 cycled in LB301 decreased significantly, indicating that serious Li/Ni mixing

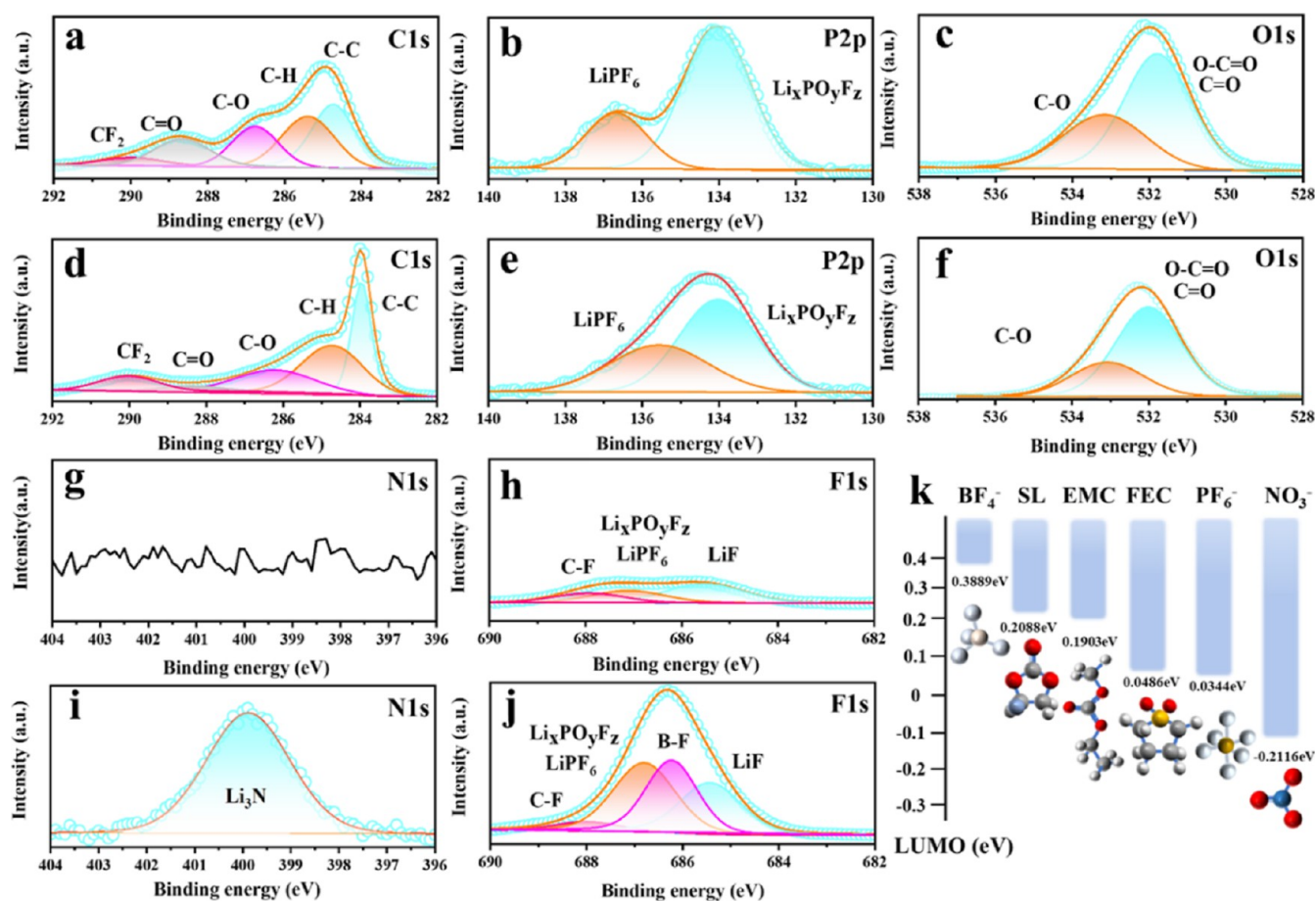


**Figure 6.** XPS of Gr electrodes employing (a–c, g,h) LB301 and (d–f, i,j) HVE after 300 cycles under 4.4 V (0.5 C). (k) LUMO energy levels calculated with DFT (25 °C).

and irreversible damage of the layered structure occurred,<sup>45</sup> whereas, the layered structure damage of the cycled NCM811 in HVE is well-alleviated, which is consistent with the TEM results. The Raman spectra of NCM811 are recorded before and after the cycle (the discharged state). Li<sup>46</sup> reported that the  $I[A_{1g}(\text{Ni})]/I[E_g(\text{Mn})]$  value of NCM material increases during the charge process (Li<sup>+</sup> deintercalation). As shown in Figure 3j, the  $I[A_{1g}(\text{Ni})]/I[E_g(\text{Mn})]$  of the cycled NCM811 in HVE is smaller than that of LB301, implying that there are more Li<sup>+</sup> re-intercalated into the NCM811 structure when cycled in HVE. The Raman results further indicate that the structural integrity of NCM811 cycled in HVE is better maintained than in LB301.

Since the irreversible phase transitions and microcrack formation usually start from the particle surface to the interior, the markedly improved performance of NCM811-Gr in HVE is likely related to the interaction of the electrolyte with the surface of NCM811. As shown in Figure 4a–c, a passivation film (CEI) is formed on the surface of NCM811 after cycling in both electrolytes. However, it is relatively thick and uneven in LB301 with a thickness of about 40 nm, while the CEI in HVE is about 20 nm and more uniform. This can indicate that HVE has a more favorable effect on the protection of the NCM811. The well-protected cathode surface in HVE facilitates uniform distribution of lithium within the bulk phase and alleviates strain and crack problems,<sup>47</sup> leading to the better electrochemical performance. The composition of CEI is investigated by XPS. The XPS results are shown in Figure 4d–

m. From the C 1s, O 1s, and F 1s spectra, it can be seen that there are more decomposition products of the solvent and LiPF<sub>6</sub> on the surface of NCM811 after cycling in LB301. The decomposition of LiPF<sub>6</sub> usually follows the formation of HF, which is detrimental to NCM811.<sup>25</sup> The CEI components in LB301 mainly include lithium alkoxides (LiOR, about 531 eV, O 1s), lithium fluoride (LiF, about 685 eV, F 1s), lithium carbonate (Li<sub>2</sub>CO<sub>3</sub>, about 532.5 eV, O 1s; about 288.5 eV, C 1s), and so forth. Although the main components of CEI in HVE are basically the same, the corresponding proportions have changed significantly, which is embodied in the obvious increase in the inorganic compounds (LiF, etc.), and significantly decline in the proportion of the solvolyzed components (lithium alkoxides, etc.). Also, the inorganic components containing B and S in the CEI of HVE are not detected in LB301. Based on the above-mentioned results, it is believed that the composition of CEI in LB301 is mainly from the decomposition of LiPF<sub>6</sub> and carbonate solvent, and that of HVE is mainly from the additive (BF<sub>4</sub><sup>-</sup>) and solvent SL. It is worth noting that the larger proportion of LiF in CEI is quite important, as LiF is known to have a wide band gap (13.6 eV) and a high oxidative stability (6.4 V vs Li/Li<sup>+</sup>).<sup>48,49</sup> Considering that LiF and inorganic components rich in B and S are more stable, they are more favorable for the protection of NCM811 and will lead to the improved Li<sup>+</sup> transmission in CEI.<sup>50,51</sup> In addition, it can also be seen from the O 1s spectrum that the M–O signal of LB301 is significantly stronger than that of HVE, which may be related

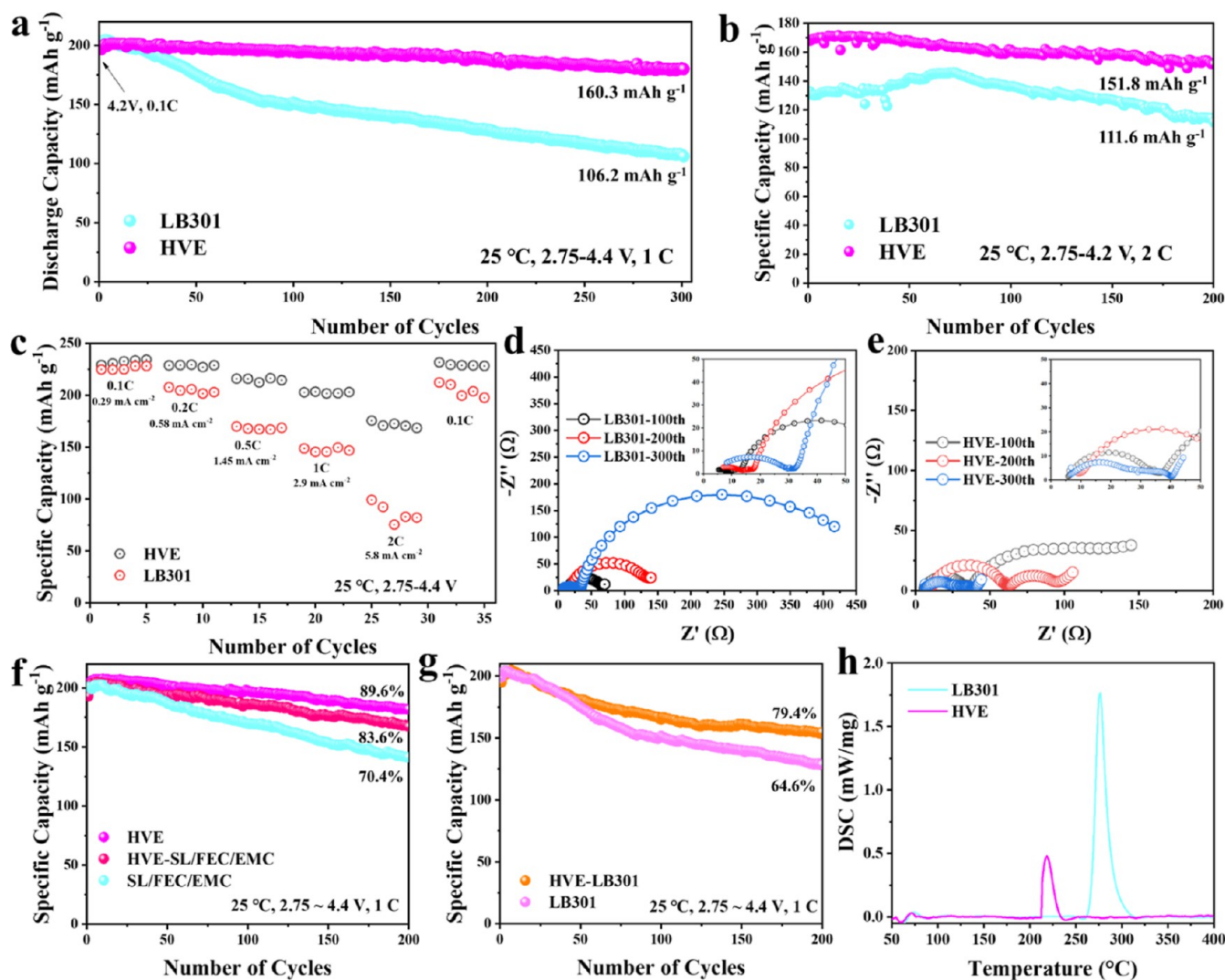


**Figure 7.** Electrochemical performance of NCM811-Gr cells employing LB301 and HVE electrolytes. Galvanostatic cycling under (a) 4.4 V at 1 C and (b) 4.2 V at 2 C. (c) Rate capability. EIS of NCM811-Gr employing (d) LB301 and (e) HVE during 300 cycles (4.4 V, 0.5 C). Galvanostatic cycling of (f) HVE-LB301 and (g) HVE-SL/FEC/EMC under 4.4 V at 1 C. (h) DSC test results of LB301 and HVE.

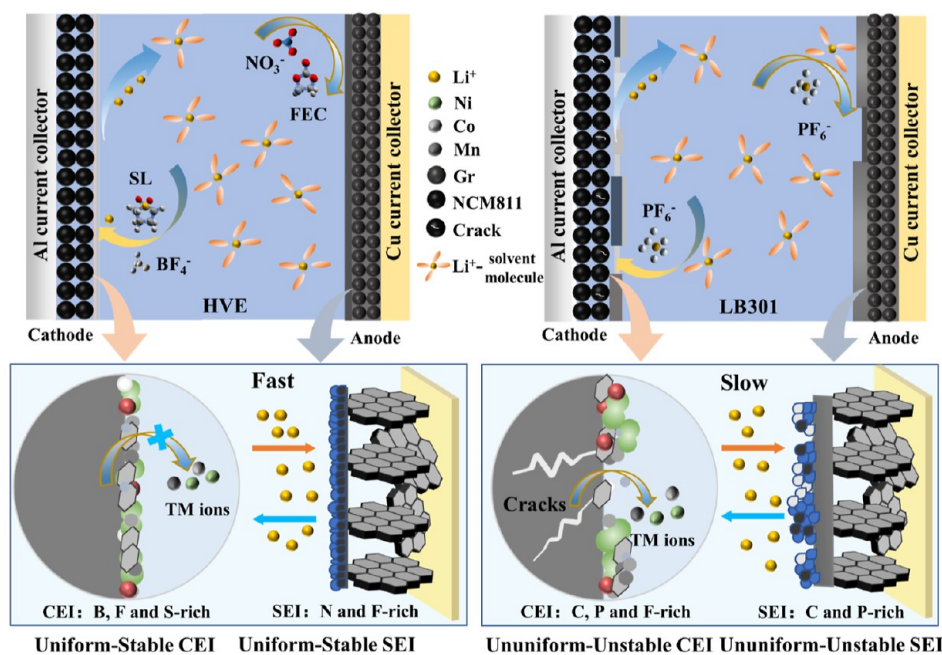
with the appearance and propagation of cracks on cycled NCM811 in LB301. Combined with the abovementioned analysis, it can be concluded that HVE can stabilize the NCM811/electrolyte interface and reduce the undesired side reactions under high voltage, thereby improving the cycle stability.

SEM images of Gr after cycling in both electrolytes are shown in Figure 5a,b,d,e. Compared with LB301, the Gr of HVE shows a smoother surface and close to the pristine. TEM images (Figure 5c,f) show that SEI is formed on the Gr surface after cycling in both electrolytes, while the SEI of LB301 is relatively thick and non-uniform, with a thickness of about 25 nm. Meanwhile, the SEI of HVE is denser and more uniform with a thickness of about 8 nm, indicating that HVE has a more favorable effect on the protection of Gr. As shown in Figure 5g,h, the XRD peak shapes of Gr after cycling in both electrolytes are basically consistent with the pristine, indicating that the overall structure does not change. It is worth noting that the (002) peak positions of both samples are shifted toward a lower angle. A previous study shows that the (002) peak of Gr shifted to a lower angle when the content of Li increased in the graphite layers.<sup>52</sup> Thus, it can be basically be

proved that there is still a part of Li remaining in Gr after 300 cycles, although in the discharged state. The larger (002) peak shift of Gr in LB301 indicates that the delithiation is more incomplete, while the shift of HVE is smaller, and the sharper (002) peak of cycled Gr in HVE than LB301 confirms the orderly and highly integrated graphitic structure, which is related to the enhanced cycle stability.<sup>18</sup> Besides, the optical photographs of cycled Gr electrodes (insets in Figure 5a,d) show that there are more dead Li on the Gr electrode surface after cycling in LB301. EDS (Figures 5i and S15) and XPS (Figure S16) are used to measure the TM ions deposited on Gr. The detected TM signals are weak for the Gr in HVE, while Mn and lots of Ni are detected on Gr of LB301. In particular, the massive deposition of Ni and Mn on Gr is thought to destroy the SEI and result in the loss of active Li and may block the diffusion path of lithium, resulting in increased resistivity of the SEI and adversely affected battery performance.<sup>19,53,54</sup>

Further XPS analysis of Gr (Figure 6a–j) reveals that the SEI components of LB301 mainly include lithium alkoxides (LiOR, ~531 eV, O 1s), decomposition products of LiPF<sub>6</sub> (Li<sub>x</sub>PO<sub>y</sub>F<sub>z</sub>, ~134 eV, P 2p), lithium fluoride (LiF), lithium

**Scheme 1. Illustration of the Mechanism of Film-Forming in HVE and LB301 and Why HVE Shows Better High-Voltage and Fast Kinetics Performance**



carbonate (Li<sub>2</sub>CO<sub>3</sub>), and so forth.<sup>20</sup> Although the main components in SEI of HVE are basically the same as LB301, the corresponding proportions have changed significantly. The alkyl carbonate components are significantly reduced. According to theoretical calculations, it can be known that NO<sub>3</sub><sup>-</sup> and FEC have relatively low LUMO values (Figure 6k). Besides, the reduction LSV (Figure S17) implies that NO<sub>3</sub><sup>-</sup> and FEC are preferentially reduced on the Gr surface. Combined with the presented experimental evidence of the increased presence of N, F-compounds in SEI, we can basically prove the preferential reduction of NO<sub>3</sub><sup>-</sup> and FEC during SEI formation. The LiF-rich SEI can sequester electrons at the SEI–Gr interface, but its poor Li<sup>+</sup> conductivity deteriorates the Li<sup>+</sup> diffusion kinetics, resulting in a larger polarization voltage and interface impedance.<sup>32,51</sup> Li<sub>3</sub>N is a fast Li<sup>+</sup> conductor that can facilitate Li<sup>+</sup> transport through the SEI.<sup>48,55</sup> Therefore, the Li<sub>3</sub>N–LiF-rich SEI not only exhibits a fast Li<sup>+</sup> transport kinetic but also effectively prevents electron penetration into SEI. Based on the abovementioned results, we believe that the SEI of LB301 is mainly derived from the decomposition products of LiPF<sub>6</sub> and carbonate solvents. However, for HVE, the additives NO<sub>3</sub><sup>-</sup> and FEC participate in the formation of SEI, and thus, the SEI of HVE mainly consists of LiF and Li<sub>3</sub>N, which are stable and more favorable for the protection of the Gr.

After elucidating the reasons for the superior stability of HVE, the comprehensive performance of HVE is further evaluated by a series of electrochemical measurements (Figures 7a,b and S18). The initial discharge specific capacities at 1 C (4.4 V) of HVE and LB301 are basically the same. However, the HVE still retains 79% of the initial discharge specific capacity after 300 cycles, while the capacity retention of LB301 is only 54%. Also, HVE still maintains a discharge specific capacity of 160.8 mA h g<sup>-1</sup> after 300 cycles under 4.2 V at 1 C, while LB301 has only 100.2 mA h g<sup>-1</sup> left. The difference of the capacity retention of HVE under 4.4 and 4.2 V is due to the different reaction reversibility. The higher voltage leads to a

higher discharge capacity as well as a severe volume change of lattice because of more Li<sup>+</sup> de-intercalation from the layered structure. Thus, NCM811 suffers more severe cracking under 4.4 V, and the expanded contact area with electrolyte will lead to more serious parasitic reaction on the cathode–electrolyte interface due to the reactive Ni<sup>4+</sup> at high SOC. Accordingly, the better reversibility of Li<sup>+</sup> de-intercalation under 4.2 V (there is less active Li loss under 4.2 V than 4.4 V) leads to the better capacity retention than 4.4 V. Especially, HVE shows a higher capacity at 2 C (4.2 V) and retains a specific discharge capacity of 151.8 mA h g<sup>-1</sup> after 200 cycles, while that of LB301 is only 111.6 mA h g<sup>-1</sup>. The rate performance of both electrolytes is shown in Figure 7c. It can be seen that the discharge specific capacity of HVE is close to that of LB301 at a low rate, while the discharge specific capacity of HVE is higher than that of LB301 at a high rate. Considering that LB301 has similar viscosity values but slightly higher conductivity than HVE, the better rate capability of HVE may be due to the fast Li<sup>+</sup> transport kinetics of the CEI and SEI,<sup>31,48</sup> which is confirmed by the XPS results. The EIS (100, 200, and 300 cycles under 4.4 V) of both samples are carried out in the discharged state. As shown in Figure 7d,e, the charge transfer impedance (*R*<sub>ct</sub>) and the overall internal resistance of LB301 are quite large and increase rapidly during the cycle, indicating that the electrode–electrolyte interfaces are not stable and fail to hinder the severe side reactions. The impedance of HVE has been relatively small, and the *R*<sub>ct</sub> even decreases during the cycle, indicating that the synergistic effect of the dual additives is indeed desirable, which is consistent with the electrochemical performance. The EIS results confirmed that the increase in internal resistance is the main reason for the capacity decline of LB301, and the smaller *R*<sub>ct</sub> (better charge transfer ability) of HVE is consistent with the better rate capability.

In order to further verify the film-forming effect of LiBF<sub>4</sub>–LiNO<sub>3</sub> dual additives, the cells pre-cycling in HVE for 3 cycles (under 4.2 V at 0.1 C) are disassembled in the Ar-glovebox.

The electrodes are rinsed with DMC and allowed to dry and then reassembled with SL/FEC/EMC or LB301. The electrochemical performance of the abovementioned cells under 4.4 V at 1 C is shown in Figure 7f,g. The HVE-SL/FEC/EMC (cells assembled with SL/FEC/EMC after pre-cycling in HVE) after 200 cycles still maintains a discharge specific capacity of 167.18 mA h g<sup>-1</sup>, superior to that of SL/FEC/EMC (155.8 mA h g<sup>-1</sup>), although not as good as HVE, and the discharge specific capacity of HVE-LB301 (cell assembled with LB301 after pre-cycling in HVE) still remains 154.8 mA h g<sup>-1</sup> after 200 cycles, while only 128.8 mA h g<sup>-1</sup> for LB301. XPS of NCM811 and Gr electrodes, which are pre-cycling in HVE and LB301, are shown in Figures S19 and S20. Compared with LB301, the surface components of both CEI and SEI in HVE contain more inorganic components (such as LiF) but less decomposition products of solvents and LiPF<sub>6</sub>. The abovementioned results suggest that LiBF<sub>4</sub>-LiNO<sub>3</sub> dual additives play a vital role in the process of film-forming and could stabilize the high-voltage NCM811-Gr full cell effectively and illustrate the importance of *in situ* generation of robust CEI and SEI, revealing that it is important to combine film-forming additives with high-voltage solvents in the development of high-voltage electrolytes. Besides, HVE shows better wettability with separator and thermal safety (smaller heat release) than LB301 (Figures S21 and 7h).<sup>56</sup>

In summary, as shown in Scheme 1, the addition of BF<sub>4</sub><sup>-</sup> and NO<sub>3</sub><sup>-</sup> dual-anion additives leads to the formation of a uniform and B-, S-, and LiF-rich CEI as well as a thin and LiN<sub>3</sub>-LiF-rich SEI. Microcracks, surface pulverization, and phase transition from layered to rock-salt of NCM811 are reduced. Meanwhile, the dissolution of TMs, the decomposition of electrolyte, and the loss of active Li are suppressed, enabling fast kinetics and reduction of overall cell impedance under high voltage. Compared with the traditional carbonate electrolyte, HVE exhibits better high-voltage and high-rate performance, illustrating the importance of *in situ* formation of high-quality CEI and SEI for the development of high-energy LIBs.

#### 4. CONCLUSIONS

Herein, an efficient electrolyte is developed to significantly improve the electrochemical and structural stability of NCM811-Gr LIBs. By combining the advantages of solvents and additives through theoretical calculation and experimental results, the high-voltage electrolyte HVE is designed, which can effectively improve the high-voltage and fast dynamics performance of Ni-rich LIBs. SL and FEC as high-voltage solvents are used to preferentially form films on the surface of cathode and anode, respectively. However, the only S-rich CEI and LiF-rich SEI could not effectively suppress the interfacial degradation under high voltage. Thus, the anion additives BF<sub>4</sub><sup>-</sup> and NO<sub>3</sub><sup>-</sup> are added to synergistically enhance the quality of CEI and SEI. Finally, a uniform and inorganic-rich CEI and a SEI enriched in inorganic compounds (LiF and Li<sub>3</sub>N) are obtained in HVE. The synergistic interaction of NO<sub>3</sub><sup>-</sup> and BF<sub>4</sub><sup>-</sup> stabilizes the electrode/electrolyte interface and promotes the fast dynamics and high-voltage performance of Ni-rich LIBs. Besides, HVE shows a better wettability with separator and acceptable thermal safety, which is beneficial to its practical use. The observed high-voltage properties show superior electrochemical performance of HVE when compared with the published literature about electrolyte for the NCM811-Gr system.<sup>14,35-41</sup> Therefore, this economical high-

voltage electrolyte may have good application prospects in commercial applications.

#### ■ ASSOCIATED CONTENT

##### Supporting Information

The Supporting Information is available free of charge at <https://pubs.acs.org/doi/10.1021/acsami.2c08724>.

SEM and electrochemical performance of NCM811 and Gr half-cells; ion conductivity and viscosity tests of LB301 and HVE; screening of high-voltage electrolytes (LSV, electrochemical performance, SEM of cycled Gr and NCM811, and EIS and optical photographs of the prepared electrolytes); normalized capacity/voltage curves; self-discharge resistance of the NCM811-Gr cells employing LB301 and HVE; slope of the RV and SV; EDS and XPS (Ni 3s spectrum and Mn 2p<sub>3/2</sub> spectrum) of cycled Gr electrodes in LB301 and HVE; galvanostatic cycling under 4.2 V at 1 C; XPS of the pre-circulated NCM811 electrode and Gr electrode employing LB301 and HVE; contact angle test results of LB301 and HVE; and Rietveld refinement results of pristine NCM811 (PDF)

#### ■ AUTHOR INFORMATION

##### Corresponding Author

Jinbao Zhao – State-Province Joint Engineering Laboratory of Power Source Technology for New Energy Vehicle, Engineering Research Center of Electrochemical Technology, Ministry of Education, College of Chemistry and Chemical Engineering, Xiamen University, Xiamen 361005, P.R. China; [orcid.org/0000-0002-2753-7508](https://orcid.org/0000-0002-2753-7508); Email: [jbzhao@xmu.edu.cn](mailto:jbzhao@xmu.edu.cn)

##### Authors

Pengpeng Dai – State-Province Joint Engineering Laboratory of Power Source Technology for New Energy Vehicle, Engineering Research Center of Electrochemical Technology, Ministry of Education, College of Chemistry and Chemical Engineering, Xiamen University, Xiamen 361005, P.R. China

Xiangbang Kong – State-Province Joint Engineering Laboratory of Power Source Technology for New Energy Vehicle, Engineering Research Center of Electrochemical Technology, Ministry of Education, College of Chemistry and Chemical Engineering, Xiamen University, Xiamen 361005, P.R. China

Huiya Yang – State-Province Joint Engineering Laboratory of Power Source Technology for New Energy Vehicle, Engineering Research Center of Electrochemical Technology, Ministry of Education, College of Chemistry and Chemical Engineering, Xiamen University, Xiamen 361005, P.R. China

Silan Kuang – State-Province Joint Engineering Laboratory of Power Source Technology for New Energy Vehicle, Engineering Research Center of Electrochemical Technology, Ministry of Education, College of Chemistry and Chemical Engineering, Xiamen University, Xiamen 361005, P.R. China

Jing Zeng – State-Province Joint Engineering Laboratory of Power Source Technology for New Energy Vehicle, Engineering Research Center of Electrochemical Technology, Ministry of Education, College of Chemistry and Chemical Engineering, Xiamen University, Xiamen 361005, P.R. China

Complete contact information is available at: <https://pubs.acs.org/10.1021/acsami.2c08724>

## Notes

The authors declare no competing financial interest.

## ACKNOWLEDGMENTS

We gratefully acknowledge the financial support of the National Natural Science Foundation of China (21875198, 22021001), the Fundamental Research Funds for the Central Universities (20720190040), the Natural Science Foundation of Fujian Province of China (2020J05009) and the key Project of Science and Technology of Xiamen (3502Z20201013). Also, we are grateful to Tan Kah Kee Innovation Laboratory (IKKEM) for help with XPS and SEM.

## REFERENCES

- (1) Jeong, M.; Lee, W.; Yun, S.; Choi, W.; Park, H.; Lee, E.; Kim, J.; Cho, S. J.; Lee, N. H.; Shin, H. J.; Yoon, W. S. Strategic Approach to Diversify Design Options for Li-Ion Batteries by Utilizing Low-Ni Layered Cathode Materials. *Adv. Energy Mater.* **2022**, *12*, 2103052.
- (2) Jiang, M.; Danilov, D. L.; Eichel, R. A.; Notten, P. H. L. A Review of Degradation Mechanisms and Recent Achievements for Ni-Rich Cathode-Based Li-Ion Batteries. *Adv. Energy Mater.* **2021**, *11*, 2103005.
- (3) Liu, J.; Wang, J.; Ni, Y.; Zhang, K.; Cheng, F.; Chen, J. Recent breakthroughs and perspectives of high-energy layered oxide cathode materials for lithium ion batteries. *Mater. Today* **2021**, *43*, 132–165.
- (4) Manthiram, A. A reflection on lithium-ion battery cathode chemistry. *Nat. Commun.* **2020**, *11*, 1550.
- (5) Yin, S. Y.; Deng, W. T.; Chen, J.; Gao, X.; Zou, G. Q.; Hou, H. S.; Ji, X. B. Fundamental and solutions of microcrack in Ni-rich layered oxide cathode materials of lithium-ion batteries. *Nano Energy* **2021**, *83*, 105854.
- (6) Zheng, H. H.; Sun, Q. N.; Liu, G.; Song, X. Y.; Battaglia, V. S. Correlation between dissolution behavior and electrochemical cycling performance for LiNi<sub>1/3</sub>Co<sub>1/3</sub>Mn<sub>1/3</sub>O<sub>2</sub>-based cells. *J. Power Sources* **2012**, *207*, 134–140.
- (7) Yan, P.; Zheng, J.; Gu, M.; Xiao, J.; Zhang, J. G.; Wang, C. M. Intragranular cracking as a critical barrier for high-voltage usage of layer-structured cathode for lithium-ion batteries. *Nat. Commun.* **2017**, *8*, 14101.
- (8) Liu, H.; Xie, Z.; Qu, W.; Dy, E.; Niketic, S.; Brueckner, S.; Tsay, K.; Fuller, E.; Bock, C.; Zaker, N.; Botton, G. A. High-Voltage Induced Surface and Intragranular Structural Evolution of Ni-Rich Layered Cathode. *Small* **2022**, *18*, No. e2200627.
- (9) Wei, W. F.; Ding, Z. P.; Chen, C.; Yang, C.; Han, B.; Xiao, L.; Liang, C. P.; Gao, P.; Cho, K. Surface-dependent stress-corrosion cracking in Ni-rich layered oxide cathodes. *Acta Mater.* **2021**, *212*, 116914.
- (10) Su, Y.; Zhang, Q.; Chen, L.; Bao, L.; Lu, Y.; Chen, S.; Wu, F. Stress accumulation in Ni-rich layered oxide cathodes: Origin, impact, and resolution. *J. Energy Chem.* **2022**, *65*, 236–253.
- (11) He, S.; Huang, S.; Zhao, Y.; Qin, H.; Shan, Y.; Hou, X. Design of a Dual-Electrolyte Battery System Based on a High-Energy NCM811-Si/C Full Battery Electrode-Compatible Electrolyte. *ACS Appl. Mater. Interfaces* **2021**, *13*, 54069–54078.
- (12) Shan, W.; Zhang, H. X.; Hu, C.; Zhou, Y.; Lam, K. H.; Wang, S. F.; Hou, X. H. The cycle performance of high nickel cathode materials significantly enhanced by the LiAlO<sub>2</sub>@Al<sub>2</sub>O<sub>3</sub> dual-modified coating. *Electrochim. Acta* **2021**, *367*, 137216.
- (13) Zhang, H. X.; Yang, S. Y.; Huang, Y. Y.; Hou, X. H. Synthesis of Non-spherical LiNi<sub>0.88</sub>Co<sub>0.09</sub>Al<sub>0.03</sub>O<sub>2</sub> Cathode Material for Lithium-Ion Batteries. *Energy Fuels* **2020**, *34*, 9002–9010.
- (14) Jang, S. H.; Jung, K.; Yim, T. Silyl-group functionalized organic additive for high voltage Ni-rich cathode material. *Curr. Appl. Phys.* **2018**, *18*, 1345–1351.
- (15) Zhang, L.; Wang, S.; Zhu, L.; He, L.; He, S.; Qin, X.; Zhao, C.; Kang, F.; Li, B. Synthesis design of interfacial nanostructure for nickel-rich layered cathodes. *Nano Energy* **2022**, *97*, 107119.
- (16) Lan, G.; Xing, L.; Bedrov, D.; Chen, J.; Guo, R.; Che, Y.; Li, Z.; Zhou, H.; Li, W. Enhanced cyclic stability of Ni-rich lithium ion battery with electrolyte film-forming additive. *J. Alloys Compd.* **2020**, *821*, 153236.
- (17) Jia, Y.; Wang, S.-N. G.; Wang, X.; Gu, L.; Dong, S. Structural Degradation of Ni-Rich Layered Oxide Cathode for Li-Ion Batteries. *J. Electrochem.* **2022**, *28*, 2108431.
- (18) Wang, Y.; Zhang, Y.; Wang, S.; Dong, S.; Dang, C.; Hu, W.; Yu, D. Y. W. Ultrafast Charging and Stable Cycling Dual-Ion Batteries Enabled via an Artificial Cathode-Electrolyte Interface. *Adv. Funct. Mater.* **2021**, *31*, 2102360.
- (19) Jung, R.; Linsenmann, F.; Thomas, R.; Wandt, J.; Solchenbach, S.; Maglia, F.; Stinner, C.; Tromp, M.; Gasteiger, H. A. Nickel, Manganese, and Cobalt Dissolution from Ni-Rich NMC and Their Effects on NMC622-Graphite Cells. *J. Electrochem. Soc.* **2019**, *166*, A378–A389.
- (20) Lin, S.; Hua, H.; Lai, P.; Zhao, J. A Multifunctional Dual-Salt Localized High-Concentration Electrolyte for Fast Dynamic High-Voltage Lithium Battery in Wide Temperature Range. *Adv. Energy Mater.* **2021**, *11*, 2101775.
- (21) Zhang, X.; Zou, L.; Xu, Y.; Cao, X.; Engelhard, M. H.; Matthews, B. E.; Zhong, L.; Wu, H.; Jia, H.; Ren, X.; Gao, P.; Chen, Z.; Qin, Y.; Kompella, C.; Arey, B. W.; Li, J.; Wang, D.; Wang, C.; Zhang, J. G.; Xu, W. Advanced Electrolytes for Fast-Charging High-Voltage Lithium-Ion Batteries in Wide-Temperature Range. *Adv. Energy Mater.* **2020**, *10*, 2000368.
- (22) Li, G.; Liao, Y.; Li, Z.; Xu, N.; Lu, Y.; Lan, G.; Sun, G.; Li, W. Constructing a Low-Impedance Interface on a High-Voltage LiNi<sub>0.8</sub>Co<sub>0.1</sub>Mn<sub>0.1</sub>O<sub>2</sub> Cathode with 2,4,6-Triphenyl Boroxine as a Film-Forming Electrolyte Additive for Li-Ion Batteries. *ACS Appl. Mater. Interfaces* **2020**, *12*, 37013–37026.
- (23) Li, S.; Li, C.; Yang, T.; Wang, W.; Lu, J.; Fan, W.; Zhao, X.; Zuo, X.; Tie, S.; Nan, J. 3,3-Diethylene Di-Sulfite (DES) as a High-Voltage Electrolyte Additive for 4.5 V LiNi<sub>0.8</sub>Co<sub>0.1</sub>Mn<sub>0.1</sub>O<sub>2</sub>/Graphite Batteries with Enhanced Performances. *ChemElectroChem* **2021**, *8*, 745–754.
- (24) Li, S.; Yang, T.; Wang, W.; Lu, J.; Zhao, X.; Fan, W.; Zuo, X.; Nan, J. 2-Thiophene sulfonamide (2-TS)-contained multi-functional electrolyte matching high-voltage LiNi<sub>0.8</sub>Mn<sub>0.1</sub>Co<sub>0.1</sub>O<sub>2</sub>/graphite batteries with enhanced performances. *Electrochim. Acta* **2020**, *352*, 136492.
- (25) Liu, M. Z.; Vatamanu, J.; Chen, X. L.; Xing, L. D.; Xu, K.; Li, W. S. Hydrolysis of LiPF<sub>6</sub>-Containing Electrolyte at High Voltage. *ACS Energy Lett.* **2021**, *6*, 2096–2102.
- (26) Markevich, E.; Salitra, G.; Aurbach, D. Fluoroethylene Carbonate as an Important Component for the Formation of an Effective Solid Electrolyte Interphase on Anodes and Cathodes for Advanced Li-Ion Batteries. *ACS Energy Lett.* **2017**, *2*, 1337–1345.
- (27) Zheng, Q.; Li, G.; Zheng, X.; Xing, L.; Xu, K.; Li, W. S. Sulfolane-Graphite Incompatibility and Its Mitigation in Li-ion Batteries. *Energy & Environmental Materials*; Wiley Online Library, **2021**; pp 1–6.
- (28) Kong, X.; Liu, J.; Zhang, Y.; Zeng, J.; Zhao, J. An effective electrolyte design to improve the high-voltage performance of high-capacity NCM811 / SiO<sub>x</sub>-Gr batteries. *Electrochim. Acta* **2020**, *349*, 136356.
- (29) Xia, J.; Nelson, K. J.; Lu, Z. H.; Dahn, J. R. Impact of electrolyte solvent and additive choices on high voltage Li-ion pouch cells. *J. Power Sources* **2016**, *329*, 387–397.
- (30) Zhao, H.; Qian, Y.; Luo, G.; Chang, J.; Wang, C.; Wang, J.; Shao, H.; Deng, Y. Cathode-anode reaction products interplay enabling high performance of LiNi<sub>0.8</sub>Co<sub>0.1</sub>Mn<sub>0.1</sub>O<sub>2</sub>/artificial graphite pouch batteries at elevated temperature. *J. Power Sources* **2021**, *514*, 230583.
- (31) Liu, Y.; Lin, D.; Li, Y.; Chen, G.; Pei, A.; Nix, O.; Li, Y.; Cui, Y. Solubility-mediated sustained release enabling nitrate additive in carbonate electrolytes for stable lithium metal anode. *Nat. Commun.* **2018**, *9*, 3656.

- (32) Cao, Z.; Hashinokuchi, M.; Doi, T.; Inaba, M. Improved Cycle Performance of LiNi<sub>0.8</sub>Co<sub>0.1</sub>Mn<sub>0.1</sub>O<sub>2</sub> Positive Electrode Material in Highly Concentrated LiBF<sub>4</sub>/DMC. *J. Electrochem. Soc.* **2019**, *166*, A82–A88.
- (33) Zuo, X. X.; Fan, C. J.; Liu, J. S.; Xiao, X.; Wu, J. H.; Nan, J. M. Lithium Tetrafluoroborate as an Electrolyte Additive to Improve the High Voltage Performance of Lithium-Ion Battery. *J. Electrochem. Soc.* **2013**, *160*, A1199–A1204.
- (34) Kuang, S.; Hua, H.; Lai, P.; Li, J.; Deng, X.; Yang, Y.; Zhao, J. Anion-Containing Solvation Structure Reconfiguration Enables Wide-Temperature Electrolyte for High-Energy-Density Lithium-Metal Batteries. *ACS Appl. Mater. Interfaces* **2022**, *14*, 19056–19066.
- (35) Becker, D.; Börner, M.; Nölle, R.; Diehl, M.; Klein, S.; Rodehorst, U.; Schmuch, R.; Winter, M.; Placke, T. Surface Modification of Ni-Rich LiNi<sub>0.8</sub>Co<sub>0.1</sub>Mn<sub>0.1</sub>O<sub>2</sub> Cathode Material by Tungsten Oxide Coating for Improved Electrochemical Performance in Lithium-Ion Batteries. *ACS Appl. Mater. Interfaces* **2019**, *11*, 18404–18414.
- (36) Feng, Z.; Rajagopalan, R.; Zhang, S.; Sun, D.; Tang, Y.; Ren, Y.; Wang, H. A Three in One Strategy to Achieve Zirconium Doping, Boron Doping, and Interfacial Coating for Stable LiNi<sub>0.8</sub>Co<sub>0.1</sub>Mn<sub>0.1</sub>O<sub>2</sub> Cathode. *Adv. Sci.* **2021**, *8*, 2001809.
- (37) Lu, J.; Li, S.; Jiang, L.; Yang, T.; Fan, W.; Wang, W.; Zhao, X.; Zuo, X.; Nan, J. Isocyanatoethyl Methacrylate (IMA) as a Bifunctional Electrolyte Additive for LiNi<sub>0.8</sub>Co<sub>0.1</sub>Mn<sub>0.1</sub>O<sub>2</sub>/Graphite Batteries with Enhanced Performance. *ChemElectroChem* **2021**, *8*, 3716–3725.
- (38) Pham, H. Q.; Thi Tran, Y. H.; Han, J.; Song, S.-W. Roles of Nonflammable Organic Liquid Electrolyte in Stabilizing the Interface of the LiNi<sub>0.8</sub>Co<sub>0.1</sub>Mn<sub>0.1</sub>O<sub>2</sub> Cathode at 4.5 V and Improving the Battery Performance. *J. Phys. Chem. C* **2019**, *124*, 175–185.
- (39) Qiu, Y.; Lu, D.; Gai, Y.; Cai, Y. Adiponitrile (ADN): A Stabilizer for the LiNi<sub>0.8</sub>Co<sub>0.1</sub>Mn<sub>0.1</sub>O<sub>2</sub> (NCM811) Electrode/Electrolyte Interface of a Graphite/NCM811 Li-Ion Cell. *ACS Appl. Mater. Interfaces* **2022**, *14*, 11398–11407.
- (40) Ran, Q.; Zhao, H.; Hu, Y.; Hao, S.; Shen, Q.; Liu, J.; Li, H.; Xiao, Y.; Li, L.; Wang, L.; Liu, X. Multifunctional Integration of Double-Shell Hybrid Nanostructure for Alleviating Surface Degradation of LiNi<sub>0.8</sub>Co<sub>0.1</sub>Mn<sub>0.1</sub>O<sub>2</sub> Cathode for Advanced Lithium-Ion Batteries at High Cutoff Voltage. *ACS Appl. Mater. Interfaces* **2020**, *12*, 9268–9276.
- (41) Yu, Z. Y.; Bai, M. H.; Song, W. F.; Hong, S.; Hong, B.; Lai, Y. Q.; Liu, Y. X. Influence of lithium difluorophosphate additive on the high voltage LiNi<sub>0.8</sub>Co<sub>0.1</sub>Mn<sub>0.1</sub>O<sub>2</sub>/graphite battery. *Ceram. Int.* **2021**, *47*, 157–162.
- (42) Xu, X.; Huo, H.; Jian, J.; Wang, L.; Zhu, H.; Xu, S.; He, X.; Yin, G.; Du, C.; Sun, X. Radially Oriented Single-Crystal Primary Nanosheets Enable Ultrahigh Rate and Cycling Properties of LiNi<sub>0.8</sub>Co<sub>0.1</sub>Mn<sub>0.1</sub>O<sub>2</sub> Cathode Material for Lithium-Ion Batteries. *Adv. Energy Mater.* **2019**, *9*, 1803963.
- (43) Harlow, J. E.; Glazier, S. L.; Li, J.; Dahn, J. R. Use of Asymmetric Average Charge- and Average Discharge- Voltages as an Indicator of the Onset of Unwanted Lithium Deposition in Lithium-Ion Cells. *J. Electrochem. Soc.* **2018**, *165*, A3595–A3601.
- (44) Ren, X. G.; Li, Y. J.; Xi, X. M.; Liu, S. W.; Xiong, Y. K.; Zhang, D. A. W.; Wang, S.; Zheng, J. C. Modification of LiNi<sub>0.8</sub>Co<sub>0.1</sub>Mn<sub>0.1</sub>O<sub>2</sub> cathode materials from the perspective of chemical stabilization and kinetic hindrance. *J. Power Sources* **2021**, *499*, 229756.
- (45) Aishova, A.; Park, G. T.; Yoon, C. S.; Sun, Y. K. Cobalt-Free High-Capacity Ni-Rich Layered Li[Ni<sub>0.9</sub>Mn<sub>0.1</sub>]O<sub>2</sub> Cathode. *Adv. Energy Mater.* **2019**, *10*, 1903179.
- (46) Li, J.; Huang, J.; Li, H.; Kong, X.; Li, X.; Zhao, J. Insight into the Redox Reaction Heterogeneity within Secondary Particles of Nickel-Rich Layered Cathode Materials. *ACS Appl. Mater. Interfaces* **2021**, *13*, 27074–27084.
- (47) Tan, S.; Shadik, Z.; Li, J.; Wang, X.; Yang, Y.; Lin, R.; Cresce, A.; Hu, J.; Hunt, A.; Waluyo, I.; Ma, L.; Monaco, F.; Cloetens, P.; Xiao, J.; Liu, Y.; Yang, X.-Q.; Xu, K.; Hu, E. Additive engineering for robust interphases to stabilize high-Ni layered structures at ultra-high voltage of 4.8 V. *Nat. Energy* **2022**, *7*, 484–494.
- (48) Zhang, X.; Jia, H.; Zou, L.; Xu, Y.; Mu, L.; Yang, Z.; Engelhard, M. H.; Kim, J.-M.; Hu, J.; Matthews, B. E.; Niu, C.; Wang, C.; Xin, H.; Lin, F.; Xu, W. Electrolyte Regulating toward Stabilization of Cobalt-Free Ultrahigh-Nickel Layered Oxide Cathode in Lithium-Ion Batteries. *ACS Energy Lett.* **2021**, *6*, 1324–1332.
- (49) Richards, W. D.; Miara, L. J.; Wang, Y.; Kim, J. C.; Ceder, G. Interface Stability in Solid-State Batteries. *Chem. Mater.* **2015**, *28*, 266–273.
- (50) Wu, F. L.; Fang, S.; Kuenzel, M.; Mullaliu, A.; Kim, J. K.; Gao, X. P.; Diemant, T.; Kim, G. T.; Passerini, S. Dual-anion ionic liquid electrolyte enables stable Ni-rich cathodes in lithium-metal batteries. *Joule* **2021**, *5*, 2177–2194.
- (51) Wu, D. X.; He, J.; Liu, J. D.; Wu, M. G.; Qi, S. A.; Wang, H. P.; Huang, J. D.; Li, F.; Tang, D. L.; Ma, J. M. Li<sub>2</sub>CO<sub>3</sub>/LiF-Rich Heterostructured Solid Electrolyte Interphase with Superior Lithiophilic and Li<sup>+</sup>-Transferred Characteristics via Adjusting Electrolyte Additives. *Adv. Energy Mater.* **2022**, *12*, 2200337.
- (52) Zhou, J.; Ma, K.; Lian, X.; Shi, Q.; Wang, J.; Chen, Z.; Guo, L.; Liu, Y.; Bachmatiuk, A.; Sun, J.; Yang, R.; Choi, J. H.; Rummeli, M. H. Eliminating Graphite Exfoliation with an Artificial Solid Electrolyte Interphase for Stable Lithium-Ion Batteries. *Small* **2022**, *18*, No. e2107460.
- (53) Heenan, T. M. M.; Wade, A.; Tan, C.; Parker, J. E.; Matras, D.; Leach, A. S.; Robinson, J. B.; Llewellyn, A.; Dimitrijevic, A.; Jervis, R.; Quinn, P. D.; Brett, D. J. L.; Shearing, P. R. Identifying the Origins of Microstructural Defects Such as Cracking within Ni-Rich NMC811 Cathode Particles for Lithium-Ion Batteries. *Adv. Energy Mater.* **2020**, *10*, 2002655.
- (54) Xu, H.; Li, Z.; Liu, T.; Han, C.; Guo, C.; Zhao, H.; Li, Q.; Lu, J.; Amine, K.; Xiu, X. Impact of Dissolved Ni<sup>2+</sup> on Solid Electrolyte Interphase of Graphite Anode. *Angew. Chem., Int. Ed.* **2022**, *61*, No. e202202894.
- (55) Piao, N.; Liu, S.; Zhang, B.; Ji, X.; Fan, X.; Wang, L.; Wang, P.-F.; Jin, T.; Liou, S.-C.; Yang, H.; Jiang, J.; Xu, K.; Schroeder, M. A.; He, X.; Wang, C. Lithium Metal Batteries Enabled by Synergistic Additives in Commercial Carbonate Electrolytes. *ACS Energy Lett.* **2021**, *6*, 1839–1848.
- (56) Xie, Q.; Cui, Z.; Manthiram, A. Unveiling the Stabilities of Nickel-Based Layered Oxide Cathodes at an Identical Degree of Delithiation in Lithium-Based Batteries. *Adv. Mater.* **2021**, *33*, 2100804.